PHYSICAL REVIEW C VOLUME 31, NUMBER 3 MARCH 1985

Decay of thermally emitted n-p states: A means to measure their lifetime

M. A. Bernstein and W. A. Friedman
Physics Department, University of Wisconsin, Madison, Wisconsin 53706
(Received 18 October 1984)

The evaporation and subsequent decay of n-p states (especially $^2H^*$—the singlet deuteron) from compound nuclei is examined theoretically. The energy difference between a proton and neutron observed in coincidence provides information about the time interval between the thermal emission and the breakup of the n-p state. It thus offers the opportunity for measuring a lifetime of the order of 10^{-21} seconds, without recourse to the relation $\Delta t = \hbar/\Gamma$. Thermal emission of both singlet and triplet deuterons is considered. The subsequent decay through the natural mode and polarization mode is calculated. Results of Monte Carlo calculations are presented for both coincidence and singles spectra, and the feasibility of direct lifetime measurement is discussed.

I. INTRODUCTION

In an earlier paper[1] we considered the process involving the evaporation and subsequent decay of $^2H^*$ (the singlet deuteron), and outlined some of the effects that this process has on the observable spectra of resulting protons and neutrons. In this paper we extend the treatment of this process. The improvements introduced are primarily concerned with the study of the time at which the two-nucleon decay occurs, and the proper treatment of the Coulomb force before and after that decay. (In Ref. 1 it was assumed that the decay occurred far from the compound nucleus.) The refinements include a theoretical treatment of the time dependence for the natural decay of the virtual n-p state, and the calculation of the increased rate of decay arising from the Coulomb polarization of the $^2H^*$ by the field of the compound nucleus. An exact treatment of its classical Coulomb trajectory is employed to describe the proton following the decay. While most of the qualitative features discussed in Ref. 1 are preserved, these refinements considerably affect the quantitative results.

This work has two goals. First, we present a calculation against which experimental measurements can be compared to further establish the existence of the thermal emission process for unstable particles. Comparison[2] of our previous work with recent data suggests the thermal emission of ^2He already may have been observed. Our second goal is to consider an experiment which enables the measurement of an extremely short time (without using the time-energy relation $\Delta t = \hbar/\Gamma$)—the time interval between the thermal emission and breakup of the singlet deuteron, which is on the order of 10^{-21} sec. This, we suggest, can be accomplished by the measurement of an energy shift between the proton and neutron, seen in coincidence at a small separation angle.

In Sec. II we explain why refinements are required for the accurate calculation of small-angle n-p coincidence cross sections, even though the less precise method described in Ref. 1 offers a good approximation in the p-p (^2He) case. The models used to calculate decay probabilities and relative momenta spectra for the virtual state of the deuteron are outlined. We discuss the advantages of using the Monte Carlo simulation technique for such calculations. We then present the results of such a Monte Carlo simulation of the decay of evaporated $^2H^*$, which allows both natural decay and Coulomb polarization to occur. From the results of this calculation we estimate the validity of using the classical trajectory approximation for the proton after the decay.

In Sec. III we examine the "background" contribution to the coincidence cross section which arises from independently evaporated protons and neutrons. In particular, we explore which compound systems minimize this contribution. We present the results of Monte Carlo calculations for two different compound systems. We present calculated neutron-proton coincidence cross sections, and also singles spectra for protons and neutrons individually. This calculation indicates that physically interesting effects directly related to the decay time should be measurable.

As in Refs. 1 and 2, we do not include contributions to the spectra from fission, direct reactions, or any other noncompound nuclear process.

II. THE EFFECT OF THE COULOMB FIELD OF THE COMPOUND NUCLEUS

In Ref. 1 we discussed the contribution to the p-p and n-p coincidence cross sections, arising from the decay of ^2He and $^2H^*$, respectively. We illustrated that discussion with a calculation assuming the asymptotic decay of the unstable particle. This assumption is a valid approximation for the description of the decay of ^2He, but not (as we stated in Ref. 1) for a quantitative calculation of the n-p coincidence spectrum. In the latter case the Coulomb field of the compound nucleus must be considered. This field has two effects—first, it accelerates the proton away from the neutron after the decay, and second, it introduces an additional decay mode and thus facilitates the dissociation of the virtual state.

Consider the diagrams given in Fig. 1 in the following explanation of why asymptotic decay is a valid assumption for ^2He, but not $^2H^*$. Figure 1(a) is the type of ve-

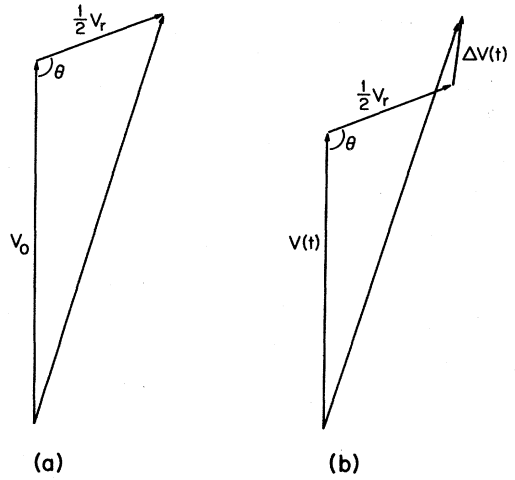

FIG. 1. Velocity diagrams (in the compound nuclear frame) for secondary protons from the decay of dinucleons. (a) The decay of the dinucleon occurred where the Coulomb field of the compound nucleus was negligible. (b) The decay of the dinucleon occurred where the field was not negligible, so the proton obtained an additional velocity $\Delta\mathbf{v}(t)$ after the decay.

locity diagram used in Ref. 1. Here we show the velocity vector for a proton, assuming the decay occurs where the field of the compound nucleus is negligible, so that the dinucleon has already obtained its asymptotic velocity $\mathbf{v}_0$. Figure 1(b) more realistically represents a decay that occurs where the field of the compound nucleus is important. In this case the center of mass of the unstable state has only obtained a speed $v(t)$ (which is less than the asymptotic speed v_0) before decay, and, after decay, the Coulomb field imparts an additional velocity $\Delta\mathbf{v}(t)$ to the proton. Considering the geometry of the orbit, one determines the direction of $\Delta\mathbf{v}(t)$ must lie between the directions of $\mathbf{v}(t)$ and $\mathbf{v}(t)+\frac{1}{2}\mathbf{v}_r$. Thus for $\frac{1}{2}v_r\sin\theta \ll v(t)$, we conclude $\Delta\mathbf{v}(t)$ and $\mathbf{v}(t)$ are nearly parallel. This condition is met by the detector geometry typically used for small-angle coincidences. Furthermore, for the case of ^{2}He decay, where the charge-to-mass ratio of each secondary particle is the same,

$$\mathbf{v}(t)+\Delta\mathbf{v}(t)\cong\mathbf{v}_0 \ . \tag{1}$$

For this reason the approximate kinematic diagram shown in Fig. 1(a) provides a good approximation for small-angle p-p coincidences arising from ^{2}He decay. In contrast, Eq. (1) is a poor approximation for ^{2}H* decay because the charge-to-mass ratios of the neutron and proton are so unequal. While it complicates the kinematics, it is precisely this feature that allows one to extract information about $\Delta\mathbf{v}(t)$, and hence about the time of the decay. Before the decay of the n-p state, the proton is accelerated and pulls the neutron along. Therefore the coincidence cross section arising from the decay of n-p states which occur well separated from the compound nucleus will be symmetric about the line $E_p=E_n$. Prompt decays, on the other hand, lead to a coincidence cross section with a maximum where E_p is greater than E_n. In the latter case, the contribution due to independently evaporated protons and neutrons is a more troublesome background, because its peak also is located such that $E_p>E_n$. We consider this background in Sec. III.

To calculate the n-p coincidence cross section we require the spectrum of relative energy which results from the decay of an isolated virtual state (called here natural decay). For this we use (as in Ref. 1) the form suggested by the Watson-Migdal formalism, but here we include the following modification: a cutoff factor of the form $\exp(-E_{\rm rel}/T)$, where T is the maximum temperature of the compound nucleus. This factor incorporates the phase space constraints imposed by the compound nucleus. (Note that this factor eliminates the need for a free parameter to cut off the unphysical portion of the Watson-Migdal expression at large values of $E_{\rm rel}$.)

Thus, for the natural decay mode we use the spectrum,

$$\frac{dN}{dE_{\rm rel}}\propto e^{-E_{\rm rel}/T}\frac{\sin^2\delta}{\sqrt{E_{\rm rel}}} \quad 0<E_{\rm rel}<\infty \ , \tag{2}$$

where δ is the $^1S_0$ n-p phase shift.

In addition to this spectrum for the natural decay, we need to know the distribution for decay times of the isolated virtual state. To obtain this, we follow Moshinsky,[3] and extract this information from the location of the poles of $S(k)$ in the complex k plane. For a true resonance, i.e., a resonance whose poles satisfy the condition $|\,\mathrm{Re}(k)\,| \gg -\mathrm{Im}(k)>0$, Moshinsky finds the well-known decay rate

$$\frac{dN(t)}{dt}=-\frac{\Gamma}{\hbar}e^{-\Gamma t/\hbar} \ , \tag{3a}$$

where Γ is the FWHM of the spectrum. His approach, however, also applies to virtual state poles. The location of the poles in this case can be obtained with the effective range expansion by setting

$$\cot(\delta)=\frac{-1}{ka}+\tfrac{1}{2}rk^2=i \ ,$$

because

$$S(k)=\exp(2i\delta)=\frac{\cot(\delta)+i}{\cot(\delta)-i} \ .$$

The resulting quadratic equation leads to poles at $k_1\cong 2i/r$ and $k_2\cong i/a$. The pole k_1 is unphysical,[4] and we have discarded it when calculating the decay curve. (Despite the fact that the unphysical pole has a small effect on the phase shift for small, real momenta, it has a larger residue, and would have dominated the calculation of the decay rate, had it been kept.)

The results of Ref. 3 for the physical pole, located at $k_2\cong i/a$, provide the following probability for a free n-p virtual state to survive until time t:

$$N(t)=|\,\mathrm{erfc}((1+i)(\zeta t)^{1/2})\,|^2 \ , \tag{3b}$$

where

$$\zeta=\frac{\hbar}{4a^2\mu}=1.87\times10^{-4}\ c/\mathrm{fm} \ .$$

The decay rate is simply found from Eq. (3b) by taking the time derivative,

$$\frac{dN(t)}{dt}=-2\left[\frac{\zeta}{\pi t}\right]^{1/2}\mathrm{Re}[e^{-2i\zeta t}(1+i)\mathrm{erfc}((1-i)(\zeta t)^{1/2})]\ . \tag{3c}$$

For large ζt, $dN(t)/dt\sim-(2\pi\zeta t^2)^{-1}$—much slower than the exponential rate of Eq. (3a).

In order to check the sensitivity of our calculations to the detailed properties of the decay rate, we calculated singles and coincidence spectra using both Eqs. (3a) and (3c). [When we use Eq. (3a), we set Γ equal to the FWHM of the spectrum in Eq. (2).] We believe that Eq. (3c) is more appropriate, and we have used this form for the sample calculations given in Sec. III. We find, however, that essentially the same spectra result when Eq. (3a) replaces (3c).

The Coulomb field of the compound nucleus introduces two important effects. It induces transitions from the deuteron ground state to the continuum, and it hastens the decay of ^{2}H* by polarizing it. We next consider these two effects. The Coulomb interaction between the compound nucleus and the proton can be expressed in terms of the distance between the proton and neutron, r, and the distance between the compound nucleus and the two-nucleon center of mass, R. R increases as the two-nucleon state recedes radially from the compound nucleus and satisfies the relation $R(t)\simeq v_0t+R_0$. In terms of these variables the Coulomb potential can be written in a Legendre expansion,

$$V(t)=\frac{Ze^2}{R(t)}\left[1+\frac{r}{2R(t)}\cos\theta_r+\cdots\right]\quad r<2R(t)$$
$$=\frac{2Ze^2}{r}\left[1+\frac{2R(t)}{r}\cos\theta_r+\cdots\right]\quad r>2R(t)\ , \tag{4}$$

where $\cos\theta_r$ gives the angle between $\mathbf{r}$ and $\mathbf{R}$, and Z is the charge of the compound nucleus. We have used a value of Z obtained from the charge of the compound nucleus averaged over the deuteron evaporation process.

First let us consider the effect of this Coulomb field on the deuteron ground state (referred to here as the triplet deuteron). It is more straightforward to evaluate the effect in this case than in the case of the virtual state (referred to here as the singlet deuteron) because the deuteron ground state has a well-studied wave function. We therefore present first a calculation of the Coulomb dissociation for the triplet deuteron. This calculation will serve both to estimate the spectra of nucleons from the breakup of the triplet deuteron, and also to illustrate some points repeated in a subsequent polarization calculation for ^{2}H*.

From time-dependent perturbation theory we have the differential transition probability,

$$\frac{d^3W_{\mathrm{dis}}(t)}{d^3\mathbf{p}}=\frac{1}{\hbar^2}\left|\int_0^t\sqrt{N(t')}\langle\psi_{\mathrm{p}}|e^{iH_0t'/\hbar}V(t')e^{-iH_0t'/\hbar}|\psi_t\rangle dt'\right|^2\ . \tag{5}$$

In Eq. (5) $\mathbf{p}$ ($=\mu\mathbf{v}_r$) is the asymptotic relative momentum for the n-p system; the operator H_0 is the n-p Hamiltonian,

$$H_0=\frac{p^2}{2\mu}+V_{\mathrm{np}}\ ;$$

$|\psi_t\rangle$ is the normalized deuteron ground state; $|\psi_{\mathrm{p}}\rangle$ is the n-p scattering state which satisfies

$$H_0|\psi_{\mathrm{p}}\rangle=\frac{p^2}{2\mu}|\psi_{\mathrm{p}}\rangle$$

and has outgoing boundary conditions; and $N(t')$ is the survival probability which decreases from its initial value $N(0)=1$, reflecting the decay of the initial state.

To evaluate the matrix element in Eq. (5), we approximate $|\psi_{\mathrm{p}}\rangle$ by the momentum eigenstate $|\mathbf{p}\rangle$; note that in the coordinate representation this eigenstate is a plane wave,

$$\langle\mathbf{r}|\mathbf{p}\rangle=\frac{\exp(\mathbf{r}\cdot\mathbf{p}/\hbar)}{(2\pi\hbar)^{3/2}}\ .$$

To be consistent, we must remember the orthogonality condition $\langle\psi_{\mathrm{p}}|\psi_t\rangle=0$. For the triplet deuteron wave function we use the zero-range approximation[5,6]

$$\langle\mathbf{r}|\psi_t\rangle=\left[\frac{\gamma}{2\pi(1-\gamma r_{0t})}\right]^{1/2}\frac{e^{-\gamma r}}{r}\ ,$$

where r_{0t} is the n-p triplet effective range. When we substitute $V(t)$ from Eq. (4) into Eq. (5) we find the contribution from the isotropic ($l=0$) term is small, and we neglect it. For simplicity, we also use the functional form of the Coulomb interaction valid for $r<2R(t)$, over the entire range of r in the integral. (This approximation causes no problem here because it leads to an *overestimate* of the differential transition probability. Even with this overestimate, however, we find the contribution to the cross sections from the deuteron ground state is negligible.) If we keep only the term in $V(t)$ proportional to $\cos\theta_r$, and substitute into Eq. (5), we find

$$\frac{d^3W_{\rm dis}(t)}{d^3\mathbf{p}}=\frac{\hbar Z^2e^4\gamma\cos^2\theta p^2}{v_0^2R_0^2\pi^2(1-\gamma r_{0t})[p^2+(\hbar\gamma)^2]^4}\times\left|\int_0^{u_m}\frac{\sqrt{N(u)}e^{i\alpha u}du}{(u+1)^2}\right|^2, \tag{6}$$

where we have introduced the dimensionless variable $u=v_0t'/R_0$. Also in Eq. (6),

$$u_m=\frac{v_0t}{R_0},$$

$$\alpha=\left[\frac{p^2}{2\mu}+B\right]\frac{R_0}{v_0\hbar},$$

B is the binding energy, and θ is defined in Fig. 1. [The factor of $\cos^2\theta$ in Eq. (6) is somewhat surprising, since it means that the proton is just as likely to be ejected towards the compound nucleus as away from it. This symmetric angular dependence is modified if higher order terms are retained in Eqs. (4) and (5), i.e., it is a property of weak fields only.]

We next consider the Coulomb polarization of the singlet deuteron. Unfortunately, we know of no standard, reliable way to evaluate the matrix element in this case. There is extensive literature[7] which describes calculations using resonant, and even virtual states, but the calculation here is especially sensitive because it involves a transition from a virtual state to another unbound state. In particular, two questions arise. The first concerns the choice of a form for the virtual state wave function. The second involves the physical significance of the $l=0$ terms in Eq. (4). With regard to the form of the wave function, we use the following approximation, which exploits our knowledge of the momentum content of the singlet deuteron in the asymptotic region. We represent this state by a packet of outgoing spherical waves, and then evaluate the matrix element of Eq. (5) in the momentum representation. Clearly the wave function is more complicated at locations inside the n-p well. Concerning the second question, we cannot invoke orthogonality to drop the $l=0$ terms in Eq. (4). However, we do drop these terms since our only interest is in transitions to states which are physically different than the initial state. Therefore we take the $l=1$ contribution to be the leading term of $V(t)$, which is the only term we use in our polarization calculation. The singlet deuteron, however, is allowed to decay into an $l=0$ state via the natural decay process.

Let the singlet deuteron wave function in the momentum representation be given by the product of a magnitude and a phase,

$$\langle\mathbf{p}\,|\,\psi_s\rangle=|\,\langle\mathbf{p}\,|\,\psi_s\rangle\,|\exp(i\phi(p)).$$

We assume that the momentum dependence of the magnitude is governed by the cutoff Watson-Migdal spectrum of Eq. (2), and take $|\,\langle\mathbf{p}\,|\,\psi_s\rangle\,|^2$ proportional to

$$\left[\frac{1}{p}\frac{dN}{dE}\right].$$

The phase, $\phi(p)$, (through its derivative, $d\phi/dp$), does affect the matrix element of Eq. (5). Brenig and Haag[8] show that this derivative has the same time delay property as the derivative of the n-p phase shift. Therefore we set $\phi(p)=\delta(p)$, where δ is the measured n-p $^1S_0$ phase shift.

To evaluate the matrix element in Eq. (5), we insert to the right of $V(t')$ the following representation of the identity operator,

$$\int\int|\,\mathbf{r}\rangle d^3r\langle\mathbf{r}\,|\,\mathbf{p}'\rangle d^3p'\langle\mathbf{p}'|.$$

The coordinate integration of this identity operator allows us to use the two different functional forms for $V(t)$ given by Eq. (4); the momentum integration allows us to use the assumed form for $\langle\mathbf{p}\,|\,\psi_s\rangle$. To evaluate the operator $\exp(iH_0t'/\hbar)$, we use the approximation

$$H_0\,|\,\mathbf{p}'\rangle\cong\frac{p'^2}{2\mu}\left|\mathbf{p}'\right\rangle.$$

Despite the approximations that we have already described, the evaluation of Eq. (5) still involves a complicated multiple integral. To calculate this quantity we follow the procedure outlined next. First we perform the integration over $d\Omega p'$, and then the integration over $d\Omega_r$. When the substitution $R'=v_0t'+R_0$ is made, the result takes the following form:

$$\frac{d^3W_{\rm dis}(t,v_0)}{d^3\mathbf{p}}=\left[\frac{4Ze^2\cos\theta}{\pi v_0\hbar}\right]^2\left|\int_{R_0}^{R(t)}dR'\sqrt{N(R')}\exp\frac{i(p^2-p'^2)(R'-R_0)}{2\mu v_0\hbar}F(R',p,p')\langle\mathbf{p}'\,|\,\psi_s\rangle p'^2dp'\right|^2, \tag{7a}$$

where the function $F(R',p,p')$ in the integrand is given by

$$F(R',p,p')=\frac{1}{\hbar^3}\left[\frac{1}{(2R')^2}\int_0^{2R'}j_0\left[\frac{p'r}{\hbar}\right]j_1\left[\frac{pr}{\hbar}\right]r^3dr+2R'\int_{2R'}^{\infty}j_0\left[\frac{p'r}{\hbar}\right]j_1\left[\frac{pr}{\hbar}\right]dr\right]. \tag{7b}$$

$F(R',p,p')$ can be evaluated in terms of the standard sine- and cosine-integral special functions, which then allows the integration over dR' to be performed analytically [when $N(R')$ is constant]. Finally, the remaining single integration over dp' must be evaluated numerically.

The most significant result of this evaluation of Eq. (5) is that the spectrum for polarized disintegration represented by Eq. (7a) is suppressed at low relative energy compared to the natural decay spectrum of Eq. (2). This suppression is due to the angular momentum barrier for the $l=1$ state of n-p relative motion. The mathematical manifestation of this barrier is the suppression, for small arguments, of the spherical Bessel function $j_1(pr/\hbar)$ [which appears in Eq. (7b)]. This effect has the practical implication that the small-angle n-p coincidence cross section is reduced by Coulomb dissociation. This, in turn, makes the experimental measurement of lifetime more difficult. An illustration of this difficulty will be presented in Sec. III.

In order to obtain the probability for a dissociative decay during a time interval Δt, we evaluate the probability difference

$$W_{\rm dis}(t+\Delta t,v_0)=W_{\rm dis}(t,v_0)\ .$$

This is obtained by integrating the differential transition probability in Eq. (7a) over d^3p at two values of the time. The integration over $d\Omega_p$ immediately gives $4\pi/3$, but the integration over dp must be done numerically. We note that the evaluation of $W_{\rm dis}(t,v_0)$ requires two numerical integrations, which must be repeated for each new value of the parameters t and v_0. Because of the large amount of computation involved, it would seem difficult to drop the simplifying assumptions that we have described earlier in this section.

The Coulomb dissociation effect we have just discussed for n-p states does not have an important effect in the p-p calculation reported in Ref. 2. This is because the Coulomb interaction for ^{2}H* given by Eq. (4) contains dipole terms, while the corresponding Coulomb energy for ^{2}He does not. Furthermore, first order perturbation theory predicts the polarization probability is proportional to Z^2. In Ref. 2, we have applied our ^{2}He formalism only to light systems, where the Coulomb effects due to the compound nucleus are smallest.

Let us next consider the calculation of the n-p coincidence cross section. In Ref. 1

$$\frac{d^4\sigma}{dE_1 d\Omega_1 dE_2 d\Omega_2}$$

was calculated from probability distributions for the dinucleon relative and c.m. energies. These energies, in addition to the Jacobian determinant, were obtained from a given pair of laboratory velocities. Because the calculations considered here also include the Coulomb orbit for the proton after dissociation, the situation is more complicated. This Coulomb orbit leads to double-valued transformation equations, i.e., there can be two sets of relative and c.m. energies for a given pair of laboratory velocities. This feature leads to singularities in the Jacobian, which complicate the numerical integration over the decay time.

The coincidence cross section, however, can be calculated with a Monte Carlo simulation, and we have chosen to use that approach here. The simulation includes the following ingredients. Singlet deuterons are isotropically "emitted" from the compound nucleus, with multiplicities and distributions of speeds in agreement with the predictions of the statistical model of Ref. 9. As a ^{2}H* recedes from the compound nucleus, time is stepped in discrete intervals, or bins. During each time bin, the ^{2}H* can decay either by the Coulomb polarization mode or the natural mode. We calculate the probabilities for these two processes independently—with no interference effects. (A similar method is used for the deuteron ground state, but of course the natural decay mode is missing.) After the decay, the Coulomb trajectory of the proton is calculated with the aid of the conserved eccentricity vector. The asymptotic proton and neutron velocities may then be transformed into the laboratory frame.

There are three major advantages to using the Monte Carlo technique. First, the kinematic transformations are single valued and there is no need for a Jacobian. Second, since the process of incrementing the time continues only until the decay occurs, the factor $N(t')$ in the integrand of Eq. (5) is always unity. Finally, any detector geometry may be modeled by the calculation.

Figure 2 shows an example of the result of the Monte Carlo calculation giving the survival probability for ^{2}H* as a function of time. The graph provides several curves. One shows the decay curve for a singlet deuteron not subject to Coulomb dissociation. The other two curves show survival probabilities in Coulomb fields of differing strengths, where the natural and polarization decay modes compete. The Coulomb dissociation probability is large—this process accounts for 37% of the decays for

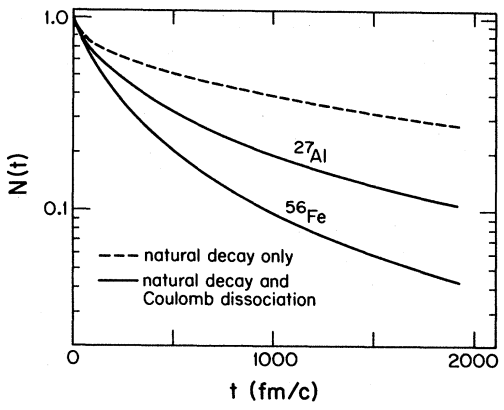

FIG. 2. The survival probability $N(t)$ of singlet deuterons as a function of time measured from the instant of thermal emission. The compound systems are formed by fusing 17 MeV/nucleon ^{14}N with ^{27}Al or ^{56}Fe. The dashed line represents the decay of the virtual state with only the natural decay channel open [see Eq. (3b)]. The solid lines show the combined effect of natural decay and Coulomb dissociation.

the reaction with the ^{27}Al target and 52% for the reaction with ^{56}Fe.

From the information in Fig. 2 we can also estimate the validity of our assumption of a classical trajectory for the proton. This approximation is best when the magnitude of the gradient of the proton's reduced wavelength, $|\nabla\lambda|$, is small. For later decay times, when local electric field varies more slowly with position [because $R(t)$ is large], and more of the energy of the proton is kinetic, the classical approximation is good. A calculation[10] of $|\nabla\lambda|$, using the decay times indicated in Fig. 2, finds that the condition $|\nabla\lambda| < 0.1$ is satisfied for about the last 80% of the decays. We thus conclude that the classical trajectory is an acceptable approximation for the two reactions considered here.

III. THE RESULTS OF SAMPLE CALCULATIONS

In Sec. II we described the qualitative effect of the finite lifetime of the singlet deuteron on the n-p coincidence cross section. In particular, we predicted a shift in the peak away from the line $E_p = E_n$, a shift which increases with decreasing lifetime. In order to extract information about the time distribution of the decays by observation of this shift, it is desirable to minimize the coincidence cross section due to independently evaporated protons and neutrons. This can be accomplished by choosing a compound system which maximizes the figure of merit defined by

$$\rho(^2\mathrm{H}^*) = \frac{N_{^2\mathrm{H}^*}}{N_p N_n} , \tag{8}$$

where the N's are the average multiplicities predicted by the statistical model of Ref. 9. (Another solution is to require the angle between the proton and neutron to be extremely small, but this would decrease the counting rate.)

In general it is hard to make $\rho(^2\mathrm{H}^*)$ large because neutrons are usually thermally emitted with a high multiplicity. Using the statistical model of Ref. 9, we find that $\rho(^2\mathrm{H}^*)$ is largest for very light compound systems. This is because the Coulomb barrier for heavy targets greatly favors emission of neutrons over charged particles. Some quantitative results are summarized in Table I. In Sec. II we also noted that heavy targets are also undesirable because the contribution of the Coulomb dissociation (which reduces the coincidence cross section) increases with increasing values of Z. If the charge of the compound nucleus is too small, however, it is also difficult to extract the interesting information about the lifetime. This is because the distance from the line $E_p = E_n$ to the expected peak of the coincidence plot is proportional to Z. If Z is too small the contribution from ^{2}H* will be nearly symmetric about this diagonal, regardless of when the decays occur. Also, the value of the coincidence cross section tends to fall with decreasing target mass, mostly because of the decreasing probability for compound nucleus formation. In order to examine the effects arising from the charge of the target, we have chosen to calculate the coincidence cross section for both a small-mass and an intermediate-mass compound system, formed by fusing 17 MeV/nucleon ^{14}N with ^{27}Al and ^{56}Fe.

TABLE I. The figure of merit $\rho(^2\mathrm{H}^*)$ [see Eq. (8)], for compound nuclear reactions induced with a ^{14}N beam.

Target \ MeV/nucleon	10	17	25
^{12}C	0.0611	0.0510	0.0459
^{27}Al	0.0376	0.0365	0.0335
^{56}Fe	0.0200	0.0214	0.0189
^{107}Ag	0.0118	0.0118	0.0117
^{197}Au	0.0121	0.0104	0.0094

In the first step of the calculation we determined the evaporation stage with the aid of the statistical model of Ref. 9. This requires a value for the Fermi energy of the compound systems as an important input parameter. We used values of 33 and 35 MeV for the mass 41 and 70 compound systems, respectively. These values are consistent with electron scattering data.[11] The statistical model then predicts, for the aluminum target, average multiplicities of $N_{^2\mathrm{H}^*} = 0.18$, $N_p = 2.0$, and $N_n = 2.4$, a maximum temperature of $T = 8.1$ MeV, and $Z = 17$ for the compound nuclear charge averaged over the evaporation process. For the iron target it predicts $N_{^2\mathrm{H}^*} = 0.16$, $N_p = 2.1$, $N_n = 3.7$, $T = 6.5$ MeV, and $Z = 30$.

We use the same method as described in Ref. 1 to calculate the background coincidence cross section due to independently evaporated protons and neutrons. We assume that these particles were isotropically emitted in the compound nuclear frame. We further assume that the background proton and neutron were thermally emitted at widely separated times, so that their final-state interactions may be neglected. Then the background coincidence cross section in the laboratory frame can be expressed as the product of the two singles spectra in the compound nuclear frame (denoted here by the subscript "s"),

$$\frac{d^4\sigma_{\text{background}}}{dE_n d\Omega_n dE_p d\Omega_p} = \sigma_0 \left[\frac{1}{4\pi}\right]^2 \left[\frac{N_p N_n - N_{^2\mathrm{H}^*}}{N_p N_n}\right] \times \left[\frac{E_p E_n}{E_{ps} E_{ns}}\right]^{1/2} \frac{dN_n}{dE_{ns}} \frac{dN_p}{dE_{ps}} , \tag{9}$$

where σ_0 is the fusion cross section.

The proton and neutron singles spectra in the compound frame are necessary ingredients for the calculation of the coincidence cross section. We calculated these singles spectra in Ref. 1 by including the secondary contribution from several unstable states, including ^{2}H*. We use the same method here, except that the secondary contribution from the breakup of n-p states has been modified to reflect their special role. The singles spectra presented here differ from those of Ref. 1 in two respects: First, they include the secondary contribution from the Coulomb-dissociated deuteron ground state, and second, the secondary contribution from both n-p states has been added in by means of a Monte Carlo calculation which includes the features discussed in Sec. II. Figure 3(a) shows this singles spectrum for protons in the compound nuclear

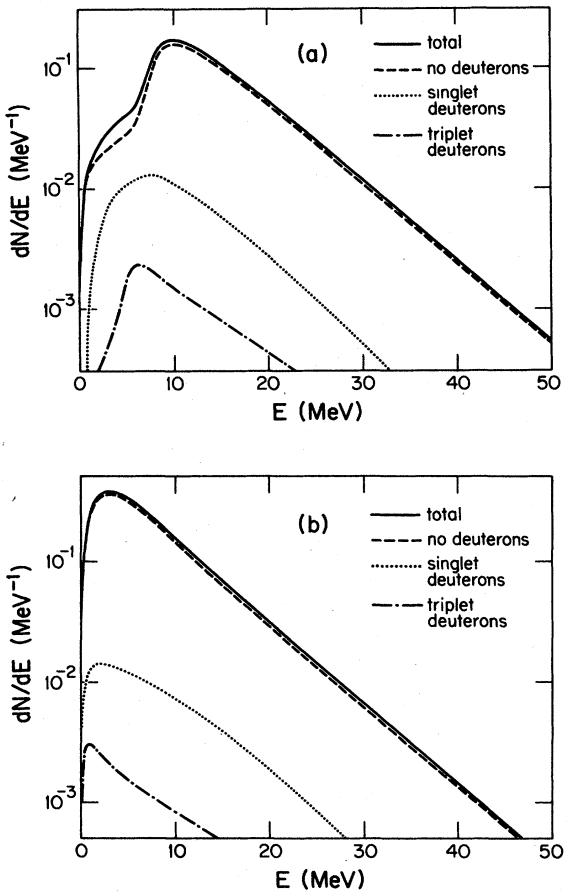

FIG. 3. Calculated singles spectra in the compound nuclear frame for (a) protons, and (b) neutrons. The compound system is formed by fusing 17 MeV/nucleon ^{14}N with ^{56}Fe. The contributions from the decay of singlet and triplet deuterons are shown. The curves marked "no deuterons" include contributions from other naturally unstable states.

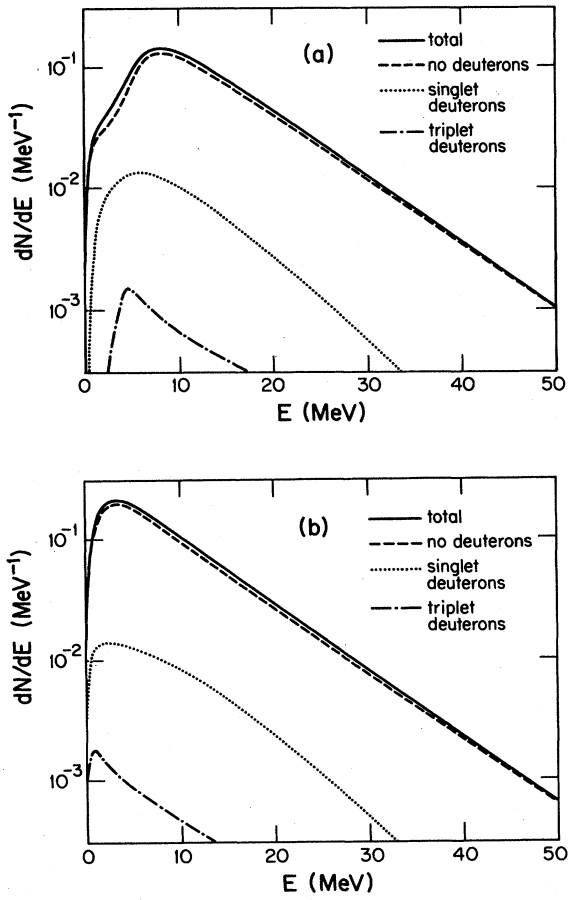

FIG. 4. Calculated singles spectra in the compound nuclear frame for (a) protons, and (b) neutrons, as in Fig. 3. The compound system is formed by fusing 17 MeV/nucleon ^{14}N with ^{27}Al.

frame for the reaction with ^{56}Fe, with the contributions from singlet and triplet deuterons separated. The area under the curve for the former is 7.0 times greater than for the latter, even though $N_{^2H^*}/N_{^2H}$ is only 0.21.

Figure 3(b) shows the singles spectrum for neutrons from the same reaction. The neutrons which come from the decay of ^{2}H* have an energy distribution almost identical to those neutrons which are evaporated in one step. This is essentially an accident, since the latter neutrons obtain a full measure of thermal energy, while the former share both thermal and Coulomb energy with the proton.

Figures 4(a) and (b) show the proton and neutron singles spectra, respectively, in the compound nuclear frame for the reaction with aluminum. Here the area under the ^{2}H* curve is 13.3 times greater than for the ^{2}H curve, and $N_{^2H^*}/N_{^2H}=0.23$. The decreased importance of ^{2}H arises from the smaller value of Z, and hence the smaller Coulomb dissociation probability.

The shift between the curves in Figs. 3(a) and (b) representing the ^{2}H* contribution does contain information about when the ^{2}H* decay occurred. This information is completely obscured, however, when the other contributions to the singles spectrum are included. Of course the coincidence technique is valuable precisely because it magnifies the ^{2}H* contribution.

To complete the calculation of the n-p coincidence cross section, we have performed a Monte Carlo calculation for the n-p coincidences arising from the decay of the ^{2}H* system. For this cross section we used a simple square "detector" with $\Delta\Omega=2.74\times10^{-3}$ sr. In order to register a coincidence, a proton and neutron from the same compound nucleus must both enter this square region. (This implies an average separation angle of $\beta\cong1.6°$.) Using this geometry, we found that the contribution from the Coulomb dissociation of ^{2}H to the coincidence cross section was even smaller than for the sin-

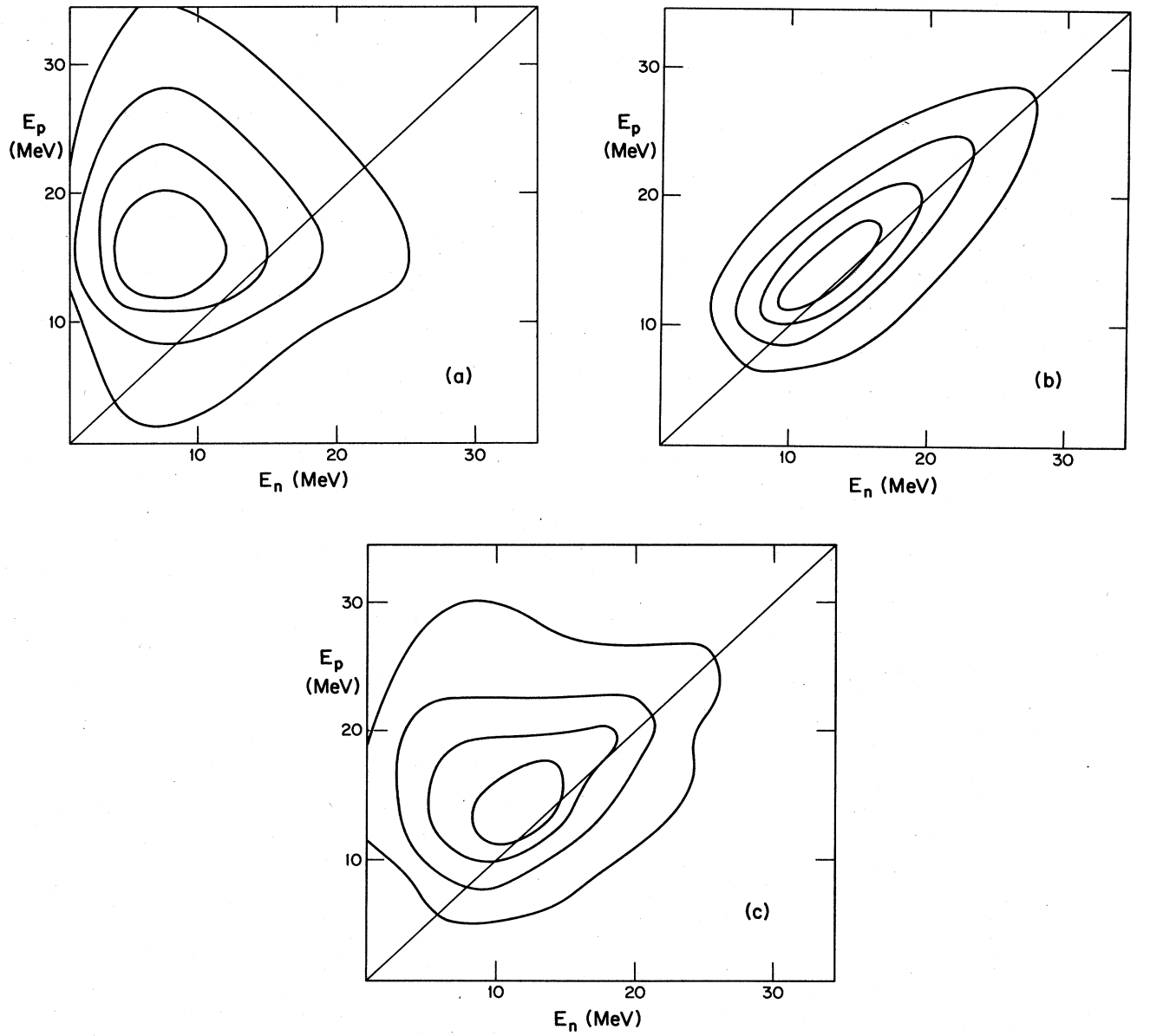

FIG. 5. Contour plots for the calculated coincidence cross section $d^4\sigma/dE_n d\Omega_n dE_p d\Omega_p$ as a function of the proton and neutron laboratory energy. The compound system is formed by fusing 17 MeV/nucleon ^{14}N with ^{27}Al. The polar angle is 30° and the detector geometry is described in the text. Each contour represents a 20% decrease in cross section. (a) The contribution from the background [see Eq. (9)]. (b) The contribution from the decay of $^2H^*$. (c) The sum of both contributions.

gles. [This is because the line shape of Eq. (6) suppresses low relative momenta.] Numerically, the contribution of ^2H, relative to that of $^2H^*$, was about an additional factor of 10 smaller than that shown in Figs. 3 and 4. Therefore we conclude that the contribution from the deuteron's ground state to the coincidence spectrum is negligible for the light and intermediate systems considered here.

The "detector" was placed at a laboratory polar angle $\theta_p=\theta_n=30°$. We chose this value because in an experiment, it would be desirable to choose the polar angle large enough to make the probability of coincidences from direct reactions small. If this angle is too large, however, the experiment would be more difficult, not only because the counting rate is diminished, but also because the laboratory energies become small.

Figure 5 shows the results of the calculation for the coincidence cross section, with the aluminum target. Figure 5(a) shows the contour map for the coincidence "background" cross section given by Eq. (9). Figure 5(b) shows the contribution to the cross section from $^2H^*$ decays. This calculated cross section was subject to statistical error because of the Monte Carlo technique. The plot is the

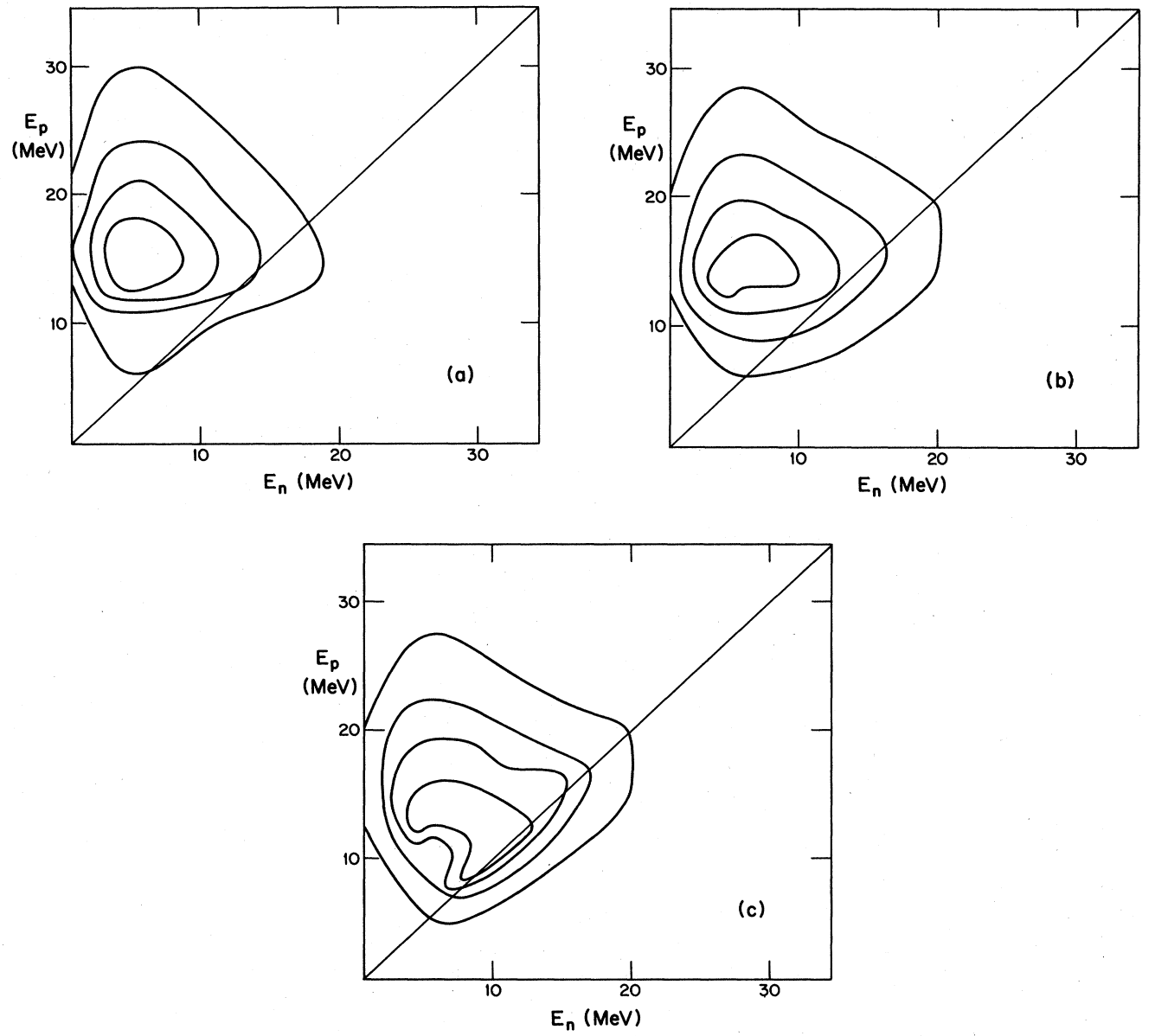

FIG. 6. Contour plots for the calculated coincidence cross section with the same beam, polar angle, detector geometry, and contour normalization as in Fig. 5. The target is ^{56}Fe. (a) The contribution from the background [see Eq. (9)]. (b) The sum of the contributions from the decay of ^{2}H*, and the background. (c) The sum of the contributions from the background and the decay of ^{2}H* with the Coulomb dissociation channel omitted.

result of a simulation of 3×10^8 compound nuclei, yielding 9478 coincidence counts. These counts were then binned into 1 MeV squares. The contours have been smoothed, and the statistical error may be estimated by noting that there were 53 counts in the bin at the peak. Figure 5(c) shows the sum of the contributions given in Figs. 5(a) and (b). If one uses a geometrical value of the fusion cross section, $\sigma_0=\pi r_0^2 A_{\text{target}}^{2/3}$, with $r_0=1.2$ fm, then the peak values in Figs. 5(a), (b), and (c) are 0.17, 0.16, and 0.29 mb/(MeV sr)^2, respectively.

Figure 6 shows the results of the calculation for the coincidence cross section, with the iron target. Figure 6(a) again shows the contour map for the coincidence "background" cross section given by Eq. (9). A comparison of Figs. 5(a) and 6(a) shows that the contours for aluminum are slightly closer to the line $E_p=E_n$, because of the reduced compound nuclear charge, Z. The contours in Fig. 5(a) also extend to higher values of the energies because of the higher speed of the compound nucleus relative to the laboratory. Figure 6(b) shows the sum of the background of Fig. 6(a) and the contribution from ^{2}H*. Unfortunately, this plot is nearly identical to that in Fig. 6(a). As we

mentioned in Sec. II, the major reason for this is the Coulomb dissociation process, which reduces the decay contribution to the small-angle coincidence cross section. To demonstrate this, Fig. 6(c) shows the sum of the background and the ^{2}H* contribution, where we have eliminated the Coulomb dissociation decay channel. The signal from ^{2}H* is now quite clear, and it is possible to extract information about the short time interval from this plot. Finally we note that the peak values in Figs. 6(a), (b), and (c) are 0.44, 0.56, and 0.58 mb/(MeV sr)^2, respectively.

As we mentioned in Sec. II, there are uncertainties with our theoretical Coulomb dissociation calculation due to the unbounded nature of ^{2}H*. If our calculation of this effect is a significant overestimate, then medium mass targets, such as iron, could be favorable. If we take the results of the Coulomb dissociation calculation as realistic, however, then the plots in Fig. 5 show that a ^{27}Al target offers a better opportunity to extract information about the time interval between the emission and decay of the ^{2}H*.

Finally we consider what can be learned about the virtual state lifetime by a direct study of the n-p coincidence cross section. If there were no background and one had contours as shown in Fig. 5(b), one could extract a measure of the difference between proton and neutron energies, ΔE, by examining the shift of the contour pattern from the symmetry line. The line which runs along the axis of the central contour region of Fig. 5(b) provides a range of 1—1.5 MeV for ΔE. From the estimate

$$\Delta E \cong \frac{Ze^2}{v_0 t_d + R_0} ,$$

it follows that $t_d \cong 2\times 10^2$ fm/c, when v_0 is taken[12] as $0.095c$ (the most likely value according to the statistical model). This value is in qualitative agreement with the underlying analysis shown in Fig. 2. The background, however, must be taken into consideration. To indicate the importance of this, we determine the "apparent" ΔE from the contours shown in Fig. 5(c) (which includes the background). This procedure gives $\Delta E \cong 3$ MeV, and hence a value of t_d approximately one-third of the true value. This illustration demonstrates that it is essential to remove the background contribution if a quantitative measure of the lifetime is to be extracted from a coincidence measurement. The background can be reduced experimentally by reducing the size of the detector.

IV. CONCLUSION

We have highlighted the differences between calculating p-p and n-p coincidence cross sections arising from the thermal emission of ^{2}He and ^{2}H*, respectively. We have shown that ^{2}H* calculation requires treatment of the polarization due to the Coulomb field of the compound nucleus. The calculations which we have presented predict that the n-p coincidence cross section is sensitive to the lifetime of the ^{2}H* virtual state. Thus a measurement of this quantity can provide a *direct* measurement of this time, which is on the order of 10^{-21} sec. We explored which compound systems allow us to extract this information most easily, by considering both a small-mass and an intermediate-mass compound nuclear system. We presented sample Monte Carlo calculations for both the coincidence and singles cross sections.

This work was supported by the National Science Foundation under Grant PHY 8204302.

[1]M. A. Bernstein, W. A. Friedman, and W. G. Lynch, Phys. Rev. C **29**, 132 (1984); **30**, 412(E) (1984).

[2]W. A. Friedman and M. A. Bernstein, Bull. Am. Phys. Soc. **28**, 973 (1983); M. A. Bernstein *et al.*, Phys. Rev. Lett. (to be published).

[3]M. Moshinsky, Phys. Rev. **84**, 525 (1951).

[4]K. W. McVoy, in *Fundamentals of Nuclear Theory,* edited by A. De-Shalit and C. Villi (International Atomic Energy Agency, Vienna, 1967), p. 463.

[5]J. M. Blatt and V. F. Weisskopf, *Theoretical Nuclear Physics* (Springer, Heidelberg, 1971), p. 611.

[6]J. Kleinfeller *et al.*, Nucl. Phys. **A370**, 205 (1981).

[7]For a partial list of references see Sec. I of W. J. Romo, J. Math. Phys. **21**, 331 (1980), and Sec. IV-A.5 of R. J. de Meijer and R. Kamermans, Rev. Mod. Phys. (to be published).

[8]W. Brenig and R. Haag, in *Quantum Scattering Theory,* edited by M. Ross (Indiana University Press, Bloomington, 1963), pp. 17 and 18 and 57—59.

[9]W. A. Friedman and W. G. Lynch, Phys. Rev. C **28**, 16 (1983).

[10]A. Messiah, *Quantum Mechanics* (Wiley, New York, 1961), Vol. I, Chap. VI, Sec. 5.

[11]E. J. Moniz *et al.*, Phys. Rev. Lett. **26**, 445 (1971).

[12]A model-independent estimate of v_0 may be extracted from the experimental singles spectra of triplet deuterons.